LA-UR- 10-00442

Approved for public release;
distribution is unlimited.

Title:	3D Thermal Modeling of TRISO Fuel Coupled with Neutronic Simulation
Author(s):	Jianwei Hu, Rizwan Uddin
Intended for:	International Congress on Advance in Nuclear Power Plants meeting

Form 836 (7/06)

3D Thermal Modeling of TRISO Fuel Coupled with Neutronic Simulation

Jianwei Hu[a,b,*], Rizwan-uddin[b]

[a]*Los Alamos National Laboratory, Los Alamos, NM, USA 87545*
[b]*Dept. of Nuclear, Plasma, and Radiological Engineering, University of Illinois at Urbana-Champaign, IL, USA 61801*

Abstract

The Very High Temperature Gas Reactor (VHTR) is widely considered as one of the top candidates identified in the Next Generation Nuclear Power-plant (NGNP) Technology Roadmap under the U.S. Department of Energy's Generation IV program. TRISO particle is a common element among different VHTR designs and its performance is critical to the safety and reliability of the whole reactor. A TRISO particle experiences complex thermo-mechanical changes during reactor operation in high temperature and high burnup conditions. TRISO fuel performance analysis requires evaluation of these changes on micro scale. Since most of these changes are temperature dependent, 3D thermal modeling of TRISO fuel is a crucial step of the whole analysis package.

In this paper, a 3D numerical thermal model was developed to calculate temperature distribution inside TRISO and pebble under different scenarios. 3D simulation is required because pebbles or TRISOs are always subjected to asymmetric thermal conditions since they are randomly packed together. The numerical model was developed using finite difference method and it was benchmarked against 1D analytical results and also results reported from literature. Monte-Carlo models were set up to calculate radial power density profile. Complex convective boundary condition was applied on the pebble outer surface. Three reactors were simulated using this model to calculate temperature distribution under different power levels. Two asymmetric boundary conditions were applied to the pebble to test the 3D capabilities. A gas bubble was hypothesized inside the TRISO kernel and 3D simulation was also carried out under this scenario. Intuition-coherent results were obtained and reported in this paper.

Keywords: thermal model, TRISO fuel, VHTR, temperature distribution

1. Introduction

As a non-emission base-load energy source, nuclear power is playing a larger role worldwide to combat global warming and secure a nation's energy supply. The Very High Temperature Gas Reactor (VHTR) is widely considered as one of the top candidates identified in the Next Generation Nuclear Power-plant (NGNP) Technology Roadmap under the U.S. Department of Energy's Generation IV program [1]. Furthermore, among the top six candidates, two reactors are given priorities, and the Very-High Temperature Reactor (VHTR) is one of them [2]. For the VHTR concept, the reactor core can be either a prismatic graphite block type core or a pebble-bed core. For the prismatic design, the cylindrical fuel compacts contain thousands of tiny TRISO particles (with a diameter of $\sim$900 μm) with graphite. And these compacts are then inserted into channels embedded in the graphite fuel assembly blocks. While for the pebble-bed design, the tennis-sized (with a diameter $\sim$6 cm) pebbles contain thousands of TRISO particles embedded in graphite as well. And these pebbles are randomly packed inside the reactor core. So the TRISO fuel particle is a common component for both designs, and it departs significantly from conventional light water fuel designs. Besides, VHTR will be operating on much higher temperature and higher burnup. Hence, to simulate TRISO fuel performance and to capture its thermo-mechanical changes on micro scale with high fidelity, multi-physics and comprehensive computer models are greatly needed. Three-dimensional heat transfer model is a crucial part of the whole package.

A tri-structural-isotropic (TRISO) particle is like a micro reactor system that has its own heat generation part and its pressure and biological containment. It has a kernel, where fissile material resides, in the center encapsulated by 4 concentric layers: a porous carbon layer (Buffer layer), an inner pyrolytic (IPyC) carbon layer, a silicon carbide (SiC) containment layer, and finally an outer pyrolytic (OPyC) carbon layer. Table 1 shows dimensions and materials of a TRISO particle. It is crucial that the TRISO particle, especially the SiC layer as it's the strongest layer, maintains its integrity during the fuel life, especially under accidental scenarios, in order to avoid/reduce release of radioactive fission fragments. So the thermal and mechanical condition of the TRISO should be closely monitored to ensure the whole reactor's safety and reliability.

During operation, nuclear reactions take place inside the TRISO kernel, and fission products are accumulated. Some of these, such as Xe, Kr and He etc., are in gaseous state. Each TRISO particle experiences complex thermo-mechanical conditions. Combined effects from several thermo-mechanical or chemical processes may lead to damage or even failure to a TRISO particle. These include pressure buildup caused by fission gas accumulation, shrinkage and creep of pyrocarbon

*Corresponding author
Email address: jhu@lanl.gov (Jianwei Hu)

caused by fast neutron irradiation, uneven thermal stresses caused by uneven thermal conditions, degradation of SiC layer caused by chemical reaction etc., and so on. Since many of these processes are temperature dependent/driven, the first step is to solve the temperature distribution inside a TRISO particle. Comparing with experiments, numerical simulation has the advantage of lower capital/time cost and high fidelity and resolution. In this work, a new 3D numerical thermal model for TRISO fuel is developed using finite difference technique, and it is benchmarked and tested in three different pebble-bed reactors. 3D simulation is required because a TRISO or pebble always has asymmetric neighboring settings since they are randomly packed together.

Pebble-bed reactors are chosen to test the code in this work. According to the Gen IV technical roadmap, three steps are necessary to pursue the VHTR concept [3]: pilot reactor, demo reactor and the full VHTR reactor. So in this work, the China HTR-10, South Africa PBMR, and the conceptual 600 MW VHTR design are chosen to represent each of the 3 stages. They differ from each other not just by size, but also by many thermal-hydraulic characteristics. Details of the 3 reactors are given in later section.

Finite difference method is used to solve the heat conduction equation in spherical geometry. TRISO particles are embedded inside graphite matrix in pebble balls, so it is natural to solve heat conduction inside pebble first. Forced-circulated helium flows through the spaces between pebbles to remove heat, so convective heat transfer boundary condition applies. Nuclear transport simulation is also needed to provide heat generation rates across a pebble or a TRISO.

2. Description: the Pebble and the TRISO

Figure 1 shows the whole picture from TRISO fuel kernel to pebble [4]. As shown in this figure, a TRISO particle is made of one kernel and 4 concentric layers. Tens of thousands of particles randomly pack inside graphite matrix to form a pebble. A pebble has a 5 mm graphite "crust". Figure 2(a) shows pebbles are stacked together [4] and Figure 2(b) shows helium flows through a pebble pile [5]. Table 1 shows dimensions, densities and thermal conductivities of each layer of TRISO. The buffer layer is made of porous carbon to hold fission gases, so its thermal conductivity is only 1/7 that of kernel. Some of the specs of TRISO are obtained from Reference [6]. Given the large number of TRISO packed inside a pebble, it is impossible to model the pebble heterogeneously. The inner part of the pebble was homogenized into a uniform fuel layer and the ratio of each material is preserved. So a pebble is modeled as two layers, the fuel layer and the crust layer. Table 2 shows dimensions, densities and thermal conductivities of the two layers of a pebble.

The thermal conductivity (λ) of the fuel layer was calculated using the empirical German relationship as shown in Equation 1 [8].

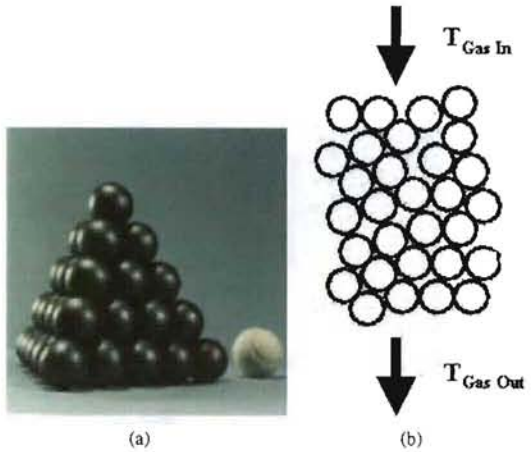

Figure 2: (a) Pile of pebbles [4]; (b) Helium flows through the space between pebbles [5].

Region	Material	Thickness (μm))	Density (g/cc)	λ ($W/(mK)$)
Kernel	14% $UC_{0.5}O_{1.5}$	250	10.5	3.5
Buffer	pourous carbon	100	1.0	0.5
IPyC	pyrolytic carbon	35	1.9	4.0
SiC	silicon carbide	35	3.2	30
OPyC	pyrolytic carbon	40	1.9	4.0

Table 1: dimensions and material characteristics of each layer of TRISO [6, 7] (λ: thermal conductivity). Note: the overall diameter of TRISO is 920 μm and its packing fraction is 0.253.

$$\lambda = 1.2768\left(\frac{-0.3906\text{E-}4T + 0.06892}{DOSIS + 1.931\text{E-}4T + 0.105} + 1.228\text{E-}4T + 0.042\right), \quad (1)$$

where λ is heat conductivity ($W/(cm\text{-}K)$), $DOSIS$ is fast neutron fluence (10^{21} n/cm^2) and T is temperature (°C). Table 3 shows selected values of λ at different T and $DOSIS$. As for the thermal conductivity of graphite, a wide range values can be found in literature. Experiment results reported by CEA [9] were chosen for the purpose of this study. Figure 3 shows variation of the thermal conductivity ($W/(m\text{-}K)$) of quasi-isotopic polycrystalline graphite as a function of neutron fluence at various irradiation temperature.

3. 1D and 3D Numerical Thermal Models for Pebble and TRISO

The purpose of developing 1D models is to benchmark the results of our numerical scheme against analytical ones. Besides, the 1D models provide quick tests for three-dimensional models. From the basic heat conservation law and Fourier's law, we have:

$$\frac{\partial}{\partial t}(\rho c T) - \nabla \cdot \lambda \nabla T = q'''(r,t), \quad (2)$$

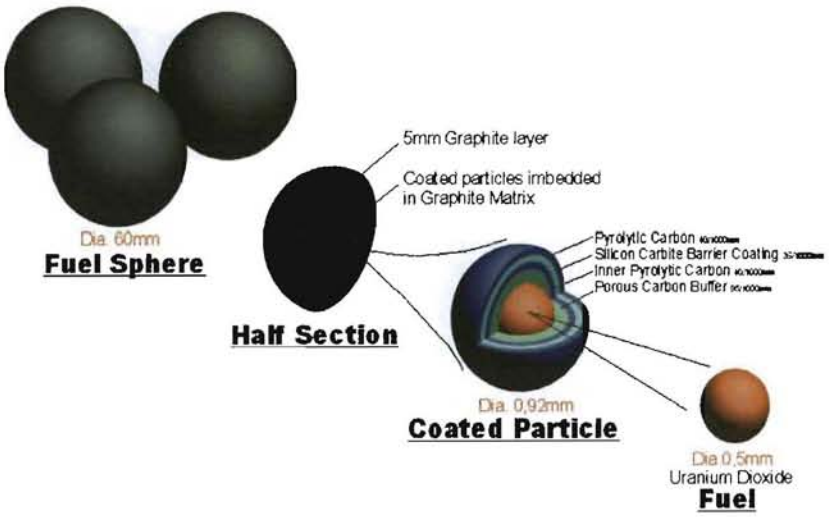

Figure 1: Fuel structure of a pebble bed reactor: different layers of TRISO and relationship between TRISO and pebble [4].

Region	Material	Radius (cm)	Density (g/cc)
Fuel	blend of TRISO and graphite	2.5	2.12
Crust	graphite	3.0	1.74

Table 2: dimensions and material characteristics of a pebble's two layers. The inner part of the pebble was homoginzed into a uniform fuel layer. Note: given the packing fraction of TRISO is 0.253, one pebble contains 40,613 TRISOs.

T (°C)	$\lambda\,(W/(cm\text{-}K))$		
	DOSIS=0	DOSIS=2.5	DOSIS=4.5
400	0.4853	0.1414	0.1307
600	0.4070	0.1687	0.1598
800	0.3613	0.1962	0.1890
1000	0.3356	0.2237	0.2182

Table 3: Selected values of the heat conductivity ($W/(cm\text{-}K)$) under different temperature and fast neutron fluence, *DOSIS* is in the unit of $10^{21} n/cm^2$.

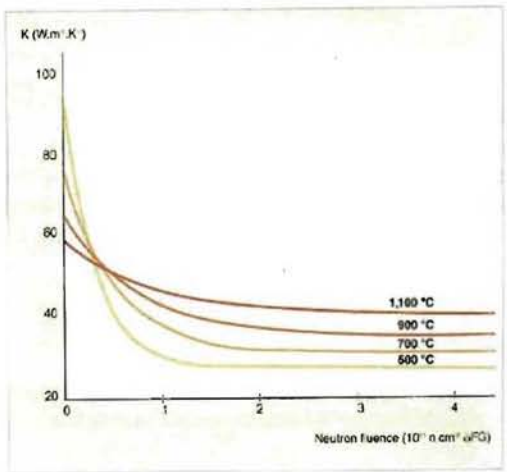

Figure 3: Variation of the thermal conductivity ($W/(m\text{-}K)$) of quasi-isotopic polycrystalline graphite as a function of neutron fluence at various irradiation temperature [9].

where $T(r,t)$ is temperature, ρ is material density, c is specific heat, q''' is volumetric heat generation.

This equation applies to both pebble and particle models. For the purpose of benchmarking in this part of the work, temporal and spatial dependence of thermal conductivity and heat generation can be ignored. The heat conduction equation at steady state is solved both analytically and numerically. Finite difference method (with central difference scheme) is used to solve the governing equation (Equation 3):

$$\frac{r_{i+\frac{1}{2}}^2 \frac{T_{i+1}-T_i}{\Delta r} - r_{i-\frac{1}{2}}^2 \frac{T_i-T_{i-1}}{\Delta r}}{r_i^2 \Delta r} = Q, \tag{3}$$

where $Q \equiv -q'''/\lambda$.

Using the numerical scheme, the temperature distribution has been calculated and compared to analytical results for a simple case. In this case, the boundary temperature is set at 800 K and the volumetric heat source is $1.19 \times 10^{10}\ W/m^3$. Figure 4 shows the comparison of analytical and numerical results. Very good agreement can be seen, showing that the numerical scheme works well. This step provides us as a stepping stone to move on to 3D numerical simulations.

As discussed earlier, 3D model is required to predict the temperature profile inside a TRISO particle or a pebble given the fact that they are always in asymmetric conditions. An analytical solution for the 3D problem is not possible because parameters such as thermal conductivity and heat generation are temperature and space dependent. The governing equation in

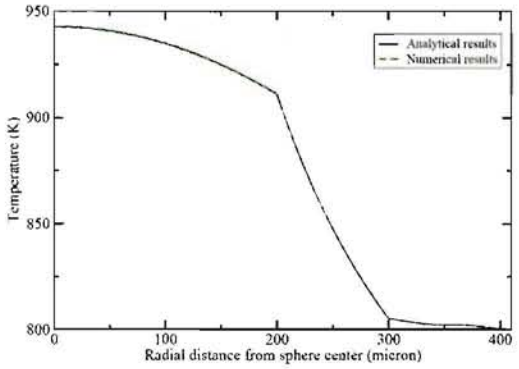

Figure 4: Radial temperature distribution across a TRISO particle, comparison of analytical and numerical results

3D spherical geometry is:

$$-r^2q'''(r) = \frac{\partial}{\partial r}\left(\lambda_f r^2 \frac{\partial T(r,\theta,\phi)}{\partial r}\right) + \frac{1}{\sin\theta}\frac{\partial}{\partial\theta}\left(\lambda_f \sin\theta \frac{\partial T(r,\theta,\phi)}{\partial\theta}\right) + \frac{1}{\sin^2\theta}\frac{\partial}{\partial\phi}\left(\lambda_f \frac{\partial T(r,\theta,\phi)}{\partial\phi}\right), \tag{4}$$

where $\lambda_f = f(T, DOSIS)$ for fuel, as shown Equation 1. At certain fuel stage, fast neutron fluence ($DOSIS$) can be assumed as constants, while temperature (T) is a function of r, θ and ϕ. So we can assume $\lambda_f = \lambda(r,\theta,\phi)$. Second-order central differences are used to discretize the equation, leading to the following equation (for brevity, $T(r_i,\theta_j,\phi_k)$ is denoted by $T(i,j,k)$ and $\lambda(r_i,\theta_j,\phi_k)$ by $\lambda(i,j,k)$):

$$-r_i^2 q_i = \frac{\lambda_{i+\frac{1}{2}} r_{i+\frac{1}{2}}^2 (T_{i+1}-T_i) - \lambda_{i-\frac{1}{2}} r_{i-\frac{1}{2}}^2 (T_i - T_{i-1})}{\Delta r^2} + \frac{\lambda_{j+\frac{1}{2}} \sin\theta_{j+\frac{1}{2}} (T_{j+1}-T_j) - \lambda_{j-\frac{1}{2}} \sin\theta_{j-\frac{1}{2}} (T_j - T_{j-1})}{\Delta\theta^2 \sin\theta_j} + \frac{\lambda_{k+\frac{1}{2}} (T_{k+1}-T_k) - \lambda_{k-\frac{1}{2}} (T_k - T_{k-1})}{\Delta\phi^2 \sin^2\theta_j}, \tag{5}$$

where

$$r_i = i\Delta r,\ \Delta r = R/L,\ i = 1,2,3,\ldots,L,$$
$$\theta_j = j\Delta\theta,\ \Delta\theta = \pi/M,\ j = 1,2,3,\ldots,M,$$
$$\phi_k = k\Delta\phi,\ \Delta\phi = 2\pi/N,\ k = 1,2,3,\ldots,N,$$
$$T_{i+1} = T(i+1,j,k),\ T_{j+1} = T(i,j+1,k),\ T_{k+1} = T(i,j,k+1),$$
$$\lambda_{i+1} = \lambda(i+1,j,k),\ \lambda_{j+1} = \lambda(i,j+1,k),\ \lambda_{k+1} = \lambda(i,j,k+1).$$

By re-arranging, we have:

$$(a_i + b_i + c_j + d_j + e_{j,k} + f_{j,k})T_{i,j,k} = a_i T_{i+1} + b_i T_{i-1} + c_j T_{j+1} + d_j T_{j-1} + e_{j,k} T_{k+1} + e_{j,k} T_{k-1} - g_i \tag{6}$$

where

$$a_i = \frac{\lambda_{i+\frac{1}{2}} r_{i+\frac{1}{2}}^2}{\Delta r^2},\ b_i = \frac{\lambda_{i-\frac{1}{2}} r_{i-\frac{1}{2}}^2}{\Delta r^2},$$
$$c_j = \frac{\lambda_{j+\frac{1}{2}} \sin\theta_{j+\frac{1}{2}}}{\Delta\theta^2 \sin\theta_j},\ d_j = \frac{\lambda_{j-\frac{1}{2}} \sin\theta_{j-\frac{1}{2}}}{\Delta\theta^2 \sin\theta_j},$$
$$e_{j,k} = \frac{\lambda_{k+\frac{1}{2}}}{\sin^2\theta_j \Delta\phi^2},\ e_{j,k} = \frac{\lambda_{k-\frac{1}{2}}}{\sin^2\theta_j \Delta\phi^2},$$
$$g_i = q_i r_i^2.$$

And values of $\lambda(i,j,k)$ can be determined by using the results of $T(i,j,k)$ from previous iteration.

As a result of the periodicity in ϕ, we have $T(i,j,N+1) = T(i,j,1)$, and $T(i,j,0) = T(i,j,N)$. Special care is needed to avoid singularity in cases of $r \to 0$, and $\theta \to 0$ or π. We denote by T_0 the common value of $T(0,j,k)$, by $T_{i,N}$ the common value of $T(i,0,k)$, and by $T_{i,S}$ the common value of $T(i,M,k)$.

For $r \to 0$ (where $\overline{\lambda}$ stands for average value),

$$T_0 = \frac{1}{MN}\sum_{j=1}^{M}\sum_{k=1}^{N} T(1,j,k) + \frac{q(\Delta r)^2}{4\overline{\lambda}(1,j,k)}. \tag{7}$$

Similarly for $\theta \to 0$ or π, we have:

$$T_{i,N} = \frac{1}{N}\sum_{k=1}^{N} T(i,1,k) + \frac{q(\Delta\theta)^2(\Delta r)^2}{4\overline{\lambda}(i,1,k)}, \tag{8}$$

$$T_{i,S} = \frac{1}{N}\sum_{k=1}^{N} T(i,M-1,k) + \frac{q(\Delta\theta)^2(\Delta r)^2}{4\overline{\lambda}(i,M-1,k)}. \tag{9}$$

For the TRISO model, $T(L,j,k)$ are known boundary values. Similar steps were taken to set up a 3D model for the pebble except that convective boundary condition applies on the outer surface.

4. Description: the Three Pebble-Bed Reactors

Boundary temperature of a TRISO particle is determined from the pebble model once its position inside the pebble is specified. For the pebble model, convective boundary conditions are needed on the outer surface. Helium flows around the surface of the ball, as shown in Figure 2(b). Rather than solving the complex helium flow problem inside the reactor, seleted data points are taken from literature. From Achenbach correlation, as suggested by Dobranich [10], the appropriate relation for Nusselt number in gas reactor is shown below:

$$Nu = Pr^{1/3}[(1.18Re^{0.58})^4 + (0.23Re^{0.75})^4]^{0.25}, \tag{10}$$

where Pr ($Pr \equiv \mu c/\lambda$) and Re ($Re \equiv \rho\overline{v_z}D_h/\mu$) are Prandtl number and Reynolds number, respectively. To determine Re, the average helium velocity ($\overline{v_z}$), the helium density (ρ) and hydraulic diameter (D_h) has to be quantified. These quantities can be calculated using the specs of reactor design. As for the dynamic viscosity (μ), the Sutherland's formula is used: $\mu =$

$u_0 \frac{T_0+C}{T+C}\left(\frac{T}{T_0}\right)^{3/2}$, where T is temperature (K) and C is Sutherland's constant. The convective heat transfer coefficient h_s can be obtained from: $h_s = \lambda Nu/D_h$.

In coherance to the 3-step strategy identified in the Gen IV technology roadmap [3], 3 representative reactors were chosen to test our codes: HTR-10, PBMR and VHTR-600. Table 4 shows the specs of the 3 reactor designs [8, 14].

Item	HTR-10	PBMR	VHTR
Thermal power (MWt)	10	268	600
Inlet temperature (°C)	250	503	600
Outlet temperature (°C)	700	908	1000
Coolant flow rate (kg/s)	3.77	126	288
Primary pressure (MPa)	3.0	7.0	7.12
Active core radius (m)	0.9	1.75	2.23
Active core height (m)	1.97	8.4	8.05
Max pebble power (W)	600	1379	2112
Mean pebble power (W)	370	612	1057

Table 4: Design specs of the 3 reactors (HTR-10, PBMR and VHTR) [8, 14].

Helium density is calculated using the *equation of state* of ideal gas, given by:

$$\rho = \frac{PM}{RT}, \tag{11}$$

where R is the gas constant (8.314 J/(K-mol)) and M is helium mol mass (4 g/mol). The hydraulic diameter (D_h) is given $D_h = d\left[\frac{2\sqrt{3}}{\pi}\left(\frac{p}{d}\right)^2 - 1\right]$ for triangular lattice [11], where p is the average distance from two neighboring pebbles (pitch) and d is pebble diameter. Pitch can be determined by using pebble packing fraction, pf, and $p = 7.184$ cm for $pf = 0.61$. And the average helium velocity ($\overline{v_z}$) can be calculated from the mass flow rate relation:

$$m_s = S_e \overline{v_z} \rho, \tag{12}$$

where m_s is mass flow rate (kg/s), S_e is effective active core cross-section area (m^2). S_e is defined as $S_e \equiv S * po$, where po is porosity of the core. The pebble packing fraction for HTR-10 is 0.61 [8], and it is assumed true for PBMR and VHTR as well. So $po = 0.39$ for all three reactors. With all the relations listed above, h_s can finally be calculated. Table 5 shows the average helium velocity ($\overline{v_z}$) and heat transfer coefficient (h_s) at inlet/outlet for each reactor.

Item	HTR-10	PBMR	VHTR
Inlet $\overline{v_z}$ (m/s)	1.5	7.738	12.047
Outlet $\overline{v_z}$ (m/s)	2.796	11.776	17.567
Inlet $\overline{h_s}$ $(W/(m^2K))$	982.47	3515.88	4321.41
Outlet $\overline{h_s}$ $(W/(m^2K))$	868.18	3244.87	4017.10

Table 5: Calculated average helium velocity ($\overline{v_z}$) and convective heat transfer coefficient ($\overline{h_s}$) at core inlet and outlet for each reactor.

5. Heat Generation Models for Pebble and TRISO

Two relatively simple models are developed to calculate the heat generation distribution in a pebble and in a TRISO particle. For thermal analysis, azimuthal variation of heat generation rate inside a pebble or TRISO is not significant, while radial variation is deemed to be important. The asymmetric 3D effects are primarily due to asymmetric boundary conditions and not so much due to asymmetry in heat generation. Rather than time-consuming whole reactor simulation, unit-cell models are set up using MCNPX [12]. Since each of the pebble ball contains thousands of TRISO particles, the fuel part of the pebble is homogenized (assuming all the materials inside the ball are blended evenly into one homogenized mixture).

For a TRISO particle, the kernel and each of the 4 coating layers are modeled explicitly. Since both TRISOs and pebbles are packed randomly together, Body-Centered-Cubes (BCC) are used to represent one pebble/TRISO with its neighbors in an average sense. And the average distance between two neighbors is determined from packing fraction. Reflective boundary conditions are used in these two models. Figure 5 shows a pebble with its neighbors, and the gap is filled with helium. The BCC model of TRISO is similar except that the gap is filled with graphite (and the dimensions would be different as well).

Criticality calculations are performed using MCNPX, and super-imposed $F6$ mesh tallies are applied to calculate fission energy and neutron/γ energy deposition in each mesh cell. Figure 6 shows normalized radial power density profile inside a TRISO particle and a pebble. In the fuel region, power density is quite uniform in both cases. For a pebble, there is enough graphite in the fuel part; while for a TRISO, its kernel size is very small comparing to neutron mean free path (in cm scale), so self-shielding is not significant in either case. In TRISO, power density is lowest in the buffer layer (250-350 μm) because of its lowest density. The power density gradient in TRISO is much higher than that in pebble because neutron can easily "flash" through the thin outer layers of TRISO without depositing energy in them.

6. Results

6.1. 1D Results of Pebble

1D model can be used to solve temperature distribution if the boundary condition can be assumed to be uniform. A test case was set up to compare this model with results in Reference [8]. In Reference [8], Gao & Shi used the full-core analysis package THERMIX developed by KFA-Julich [13], which includes several modules covering gas flow and major core components, while the fuel pebble model is one-dimensional. Table 6 shows the comparison of max fuel temperature and max fuel surface temperature between this work and Gao & Shi. In this case, the max temperature is assumed to take place where the coolant is hottest (818 °C) and the pebble power is close to maximum (0.52 kW). The results are quite close given the fact that some details are not specified in this reference.

Figure 5: MCNPX model of a pebble and its neighbors using Body-Centered-Cubes representation (reflective boundary condition applied).

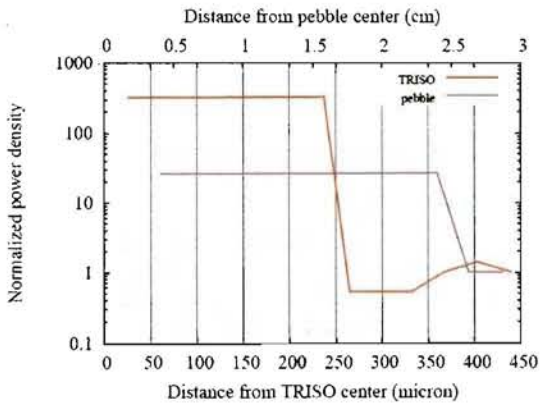

Figure 6: Normalized radial power density profile inside a TRISO particle and a pebble.

Item	this work	Gao & Shi
Max fuel temp. (°C)	917.7	918.7
Max fuel surface temp. (°C)	870.7	876.7

Table 6: Comparison of max fuel temperature and max fuel surface temperature (°C) between this work and Gao & Shi [8]. In this case, the max temperature is assumed to take place where the coolant is hottest (818 °C) and the pebble power is close to maximum (0.52 kW).

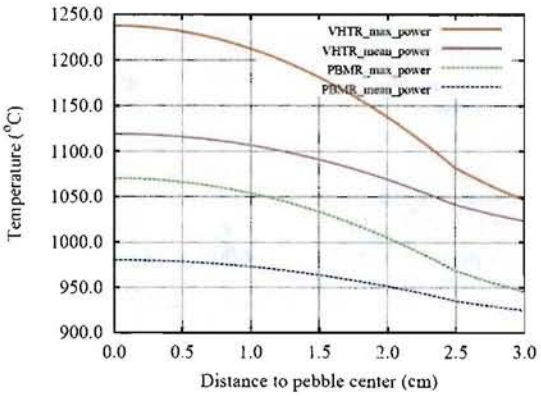

Figure 7: Radial temperature distribution across a pebble of VHTR and PBMR, each with max and mean pebble power, and the pebble is assumed close to the outlet in each reactor Table 4. Results were obtained from 1D modeling and the convective heat transfer coefficient is assumed to be h_{s0} all over.

Figure 7 shows the temperature distribution along radial distance from pebble center. It assumes that the pebble is in a symmetric condition (i.e., the helium flow is symmetric all around the pebble surface and the pebble is isotropic by itself, so the convective heat transfer coefficient is assumed to be h_{s0} all over the surface). 1D simulations were performed for four cases, PBMR pebble with max and mean power and VHTR pebble with max and mean power, as shown in Table 4, assuming the pebbles are close to outlet. The temperature gradient is smaller in the crust ($r > 2.5$ cm) because its thermal conductivity is higher than that in the fuel part. Overall temperature drop (ΔT) across the pebble for PBMR at mean and max power are 57.2 and 134.6 °C, 95.4 and 190.8 °C for VHTR respectively. Maximum temperature is 1240 and 1060 °C under max power for VHTR and PBMR respectively, and it is expected to increase under asymmetric boundary conditions or accidental scenario. Given the operating max fuel temperature is 1250 °C and accidental max is 1600 °C [8, 15] (even though these two limits might be extended in the future), the temperature inside VHTR pebble is too high. It can be alleviated by reducing power, pebble packing fraction, or increasing helium flow rate, etc.

6.2. 3D Results of Pebble

In order to test the 3D capabilities of our codes, two asymmetric boundary conditions are set up : Case 1) a pebble is sitting in a uniform one-directional helium flow, as shown in Figure 8(a); Case 2) a pebble is sitting on top of 3 other pebbles

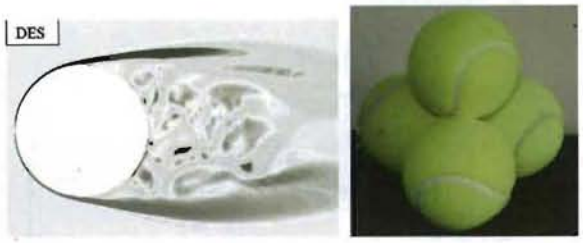

(a) Case 1 (b) Case 2

Figure 8: Two asymmetric boundary conditions: (a) Case 1, a pebble is in one-directional helium flow [16]; (b) Case 2, a pebble is sitting on top of 3 other pebbles (illustrated with tennis balls).

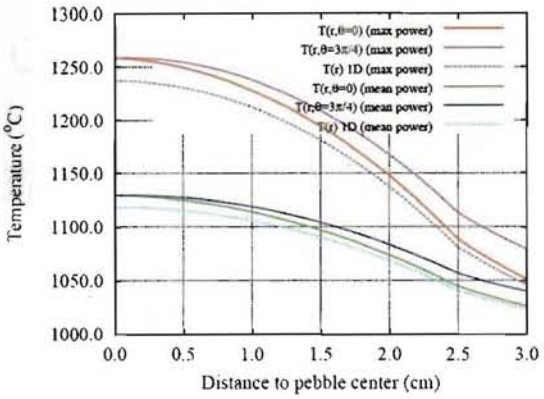

Figure 9: Radial temperature distribution across a pebble of VHTR along two different polar angles (θ) under max and mean pebble power. Results from 1D simulations are also included for comparison.

Figure 8(b). 3D modeling results of only VHTR are presented here for brevity.

For Case 1 boundary condition, it is actually a 2D problem because it can be assumed azimuthally (ϕ) symmetric. For the convenience of this study, the convective heat transfer coefficient, h_s, is assumed to decrease continuously with the polar angle (θ) from h_{s0} at the left most point ($\theta = 0$) to $0.4h_{s0}$ at the right most point ($\theta = \pi$) on the pebble surface (as shown in Figure 8(a)). (More realistic boundary condition can be fed into the code once the flow field is solved.) The governing equation (Equation 5) on a polar grid with (r, θ, ϕ) the radial, polar, and azimuthal directions, respectively. All simulations in this section were performed on a mesh of about 3 million grid nodes ($301 \times 101 \times 101$ points in the r, θ and ϕ directions).

Figure 9 shows radial temperature distribution across a VHTR pebble along two different polar angles ($\theta = 0$ and $3\pi/4$) under max and mean power. Temperature along $\theta = 3\pi/4$ is always higher than $\theta = 0$ since h_s decreases with θ. By comparing with 1D results, this asymmetric boundary condition introduced temperature rise all over the pebble, ~20 °C under max power and ~10 °C under mean power.

For Case 2 boundary condition, the top pebble has 3 contact points, which are azimuthally symmetric, on its surface (see Figure 8(b)). Since the 3 pebbles below it partially block the

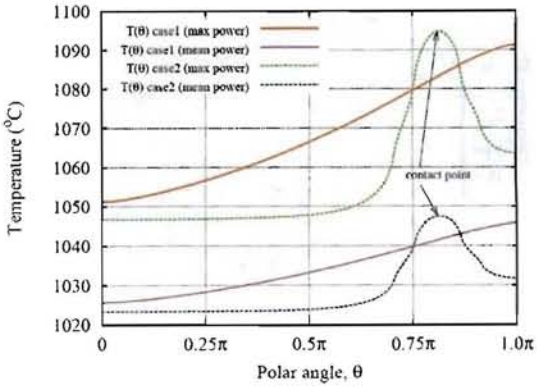

Figure 10: Temperature variation along polar angle (θ) on the pebble surface in Case 1 and Case 2. In Case 1, it is the azimuthally averaged temperature; while in Case 2, it is the temperature along θ for a fixed ϕ.

helium flow, lower helium velocities are expected in area surrounding the "south pole" ($\theta = \pi$, the lowest point on the top pebble as shown in Figure 8(b)). This code can take different h_s on every surface grid point if the complex helium flow is solved. For the purpose of this study, simplified h_s is set as following ($\theta_0 = 0.81\pi$):

$$h_s = \begin{cases} 0, & \text{small ring around the contact points}(r < 0.5cm) \\ 0.5h_{s0}, & \text{the area a little farther}(0.5cm < r < 1cm) \\ 0.8h_{s0}, & \text{other area } \theta > \theta_0 \text{ (on contact points } \theta = \theta_0) \\ h_{s0}, & \text{the rest of the pebble surface.} \end{cases}$$

Figure 10 shows temperature variation along polar angle (θ) on the pebble surface in Case 1 and Case 2, each with mean and max pebble power. In Case 1, it is the azimuthally averages temperature; while in Case 2, it is the temperature along θ for a fixed ϕ. For Case 1, it shows a clear trend that the pebble surface temperature rises along θ, since h_s decreases continuously along θ. The max temperature difference on the surface is ~40°C and ~20°C at max and mean power respectively. For Case 2, a significant "bump" in temperature can be seen around the contact point ($\theta = \theta_0$ (0.81π)), and the temperature also rises after the contact points because of the poor cooling conditions around the contact points and in area the under the contact points ($\theta > \theta_0$).

Figure 11 shows temperature variation as a function of r and ϕ (with θ fixed at θ_0). It basically shows the temperature on the cone of $\theta = \theta_0$ (which goes through the pebble center and all 3 contact points). Three "bumps" can be seen on the right edge of the surface plot, where the contact points reside. The influence of the contact points dies away in regions farther beneath the surface ($r < 2$ cm). The surface temperature increases dramatically on hot spots, although the pebble center temperature increases only ~10°C caused by this asymmetric boundary condition.

6.3. 3D Results of TRISO

A 3D test case was also developed for TRISO: a gas bubble was assumed to exist in the TRISO kernel, and it is centered at

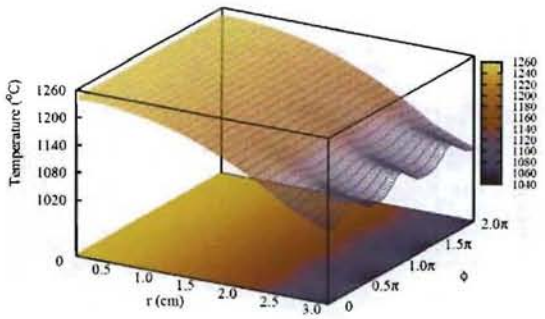

Figure 11: Temperature variation of a pebble as a function of r and ϕ with θ fixed at θ_0. It basically shows the temperature on the cone of $\theta = 0.81\pi$ (which goes through the pebble center and all 3 contact points on the surface).

($r = 125\ \mu$m, $\theta = \pi/4$, $\phi = \pi/2$). Its radius is assumed to be a quarter that of kernel ($0.25r_0$). Since the gas bubble contains mainly Xe, Kr and He, its heat conductivity is low (assumed to be $0.02\ W/(mK)$). There is no fission reaction taking place in it so its heat generation is assumed zero. Temperature on the TRISO outer surface is set as 900 °C (more accurate boundary condition can be set once its exact location inside the pebble is determined). Figure 12 shows temperature variation along radial distance from TRISO center at 3 different polar angle ($\theta = 0$, $\pi/4$, *or* $3\pi/4$, and ϕ is fixed at 0.5π). The temperature drop over the whole TRISO is ~13 °C, and it mainly occurs in the kernel and buffer layer because the kernel has high heat source and the buffer has much lower thermal conductivity. The temperature gradient is significant given the TRISO radius is only 460 μm. The temperature has a "dip" inside kernel along $\theta = \pi/4$ by comparing the other two curves, because $\theta = \pi/4$ runs right through the gas bubble. The effect of zero heat source in the bubble overtakes that of its low heat conductivity, thus it makes its temperature lower. Temperature along $\theta = 3\pi/4$ is not affected by the bubble since it is farther from it. Figure 13 shows the temperature variation of a TRISO as a function of r and ϕ (with θ fixed at $\pi/4$). As shown, temperature along $\phi = 0.5\pi$ is lower than that along other azimuthal angle since the gas bubble is centered at ($r = 125\ \mu$m, $\theta = \pi/4$, $\phi = \pi/2$). The presence of the gas bubble does not only affect temperature within it but region immediate "down stream", because no heat generated inside bubble thus it has smaller heat flux after it.

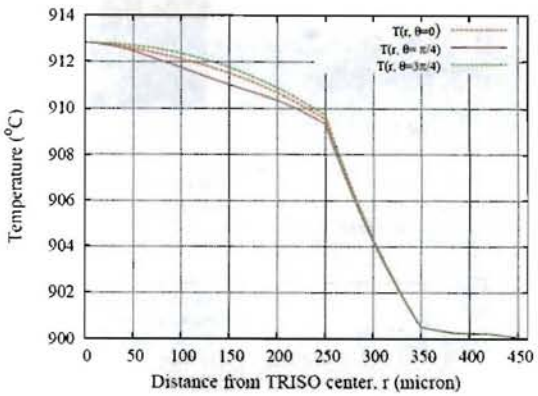

Figure 12: Temperature variation along radial distance from TRISO center at 3 different polar angle ($\theta = 0$, $\pi/4$, *or* $3\pi/4$, and ϕ is fixed at 0.5π).

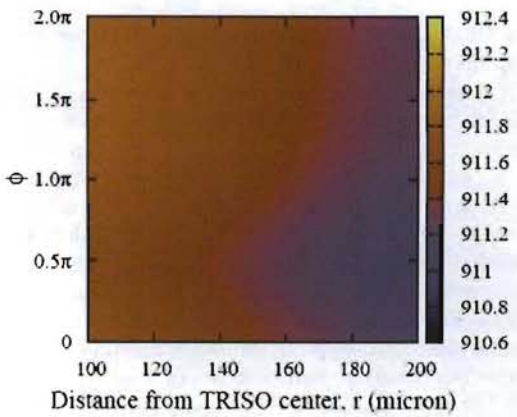

Figure 13: Temperature variation of a TRISO as a function of r and ϕ with θ fixed at $\pi/4$. As shown, temperature along $\phi = 0.5\pi$ is lower than other azimuthal angle since the gas bubble is centered at ($r = 125\ \mu$m, $\theta = \pi/4$, $\phi = \pi/2$).

Summary

A TRISO particle experiences complex thermo-mechanical changes during reactor operation in high temperature and high burnup conditions. TRISO fuel performance analysis requires evaluation of these changes on micro scale. Since most of these changes are temperature dependent, 3D thermal modeling of TRISO fuel is a crucial part of the whole analysis package. In this paper, 3D numerical model has been developed using finite difference techniques. Special care has been taken at certain points to avoid singularity. Since TRISO particles are embedded inside pebbles for pebble-bed reactor design, 3D models are also developed for pebbles. Complex boundary conditions with

convective heat transfer has been studied and applied on pebble outer surface. Results from this numerical model have been compared with analytical results and also with reported results of HTR-10 from literature, and good agreements are obtained. Monte-Carlo models have been developed and heat generation along radial distance inside a TRISO and a pebble have been calculated. 3D thermal simulations have been performed with three reactors (HTR-10, PBMR and VHTR). Maximum temperature is 1240 and 1060 °C under max power for VHTR and PBMR respectively, and it is expected to increase under asymmetric boundary conditions or accidental scenario. So modification of VHTR design is needed to make sure max fuel temperature is below 1250 °C. Two asymmetric boundary conditions are added to the pebble model to further test the 3D capabilities of the code. Higher temperature was observed in the center and in affected regions. Results agree with intuition, though further validations are required. A gas bubble was hypothesized inside the TRISO kernel and 3D simulation was carried out under this scenario. Lower temperature was seen inside the bubble and in region immediate "down stream". Future work will focus on integrating this thermal model into the TRISO fuel performance package. Results from thermal modeling will be fed into gas migration and stress analysis, feedback from which will also provide inputs for more accurate thermal analysis as well. In short, this work is a stepping stone for the whole fuel performance analysis effort.

Acknowledgements

The authors would like to thank Dr. Stephen Tobin, Dr. Hashem Mourad and Dr. Michael Fensin for their continued support and valuable inputs on this work.

References

[1] *A Technology Roadmap for Generation IV Nuclear Energy Stystems*, Issued by U.S. DOE nuclear energy research advisory committee and the Geneneration IV international forum (Dec. 2002).

[2] *U.S. Generation IV Priorities*, http://www.ne.doe.gov/genIV/neGenIV4.html (2009).

[3] *Generation IV Roadmap, R&D Scope Report for Gas-Cooled Reactor Systems*, Issued by U.S. DOE nuclear energy research advisory committee and the Geneneration IV international forum (2002).

[4] D. Petti, W. Windes, "Fuel and Graphite Needs for VHTR," *talk on the Advanced Test Reactor National Scientific User Facility Users Week 2009*, Idaho National Laboratory (2009).

[5] J. Wang, R.G. Ballinger, and H.J. Maclean, "TIMCOAT: an Integrated Fuel Performance Model for Coated Particle Fuel," *Nucl. Tech.*, 148:68 (2004).

[6] J.W. Sterbentz, B. Phillips, R.L. Sant, G.S. Chang, and P.D. Bayless, *Reactor Physics Parametric and Depletion Studies in Support of TRISO Particle Fuel Specification for the Next Generation Nuclear Plant*, INEEL/EXT-04-02331 (2004).

[7] D. Petti, A. Languille, P. Martin, and R.G. Ballinger, *Development of Improved Models and Designs for Coated-particle Gas Reactor Fuels*, INEEL/EXT-02-01493 (2002).

[8] Zuiying Gao and Lei Shi, "Thermal Hydraulic Calculation of the HTR-10 for the Initial and Equilibrium Core," *Nucl. Eng. and Des.*, **218**, 51-64 (2002).

[9] Gas-cooled Nuclear Reactors, Issued by Commissariat a lenergie atomique (CEA), 30, ISBN 2-281-11343-4.

[10] D. Dobranich, *Heat transfer and thermal stress analysis of the multilayered spherical particles of a Particle Bed Space Reactor. PhD thesis*, SAND90-1032, Sandia National Laboratories (1991).

[11] J.J. Duderstadt, L.J. Hamilton, *Nuclear Reactor Analysis*, 485, John Wiley & Sons (1992).

[12] *MCNPX USER'S MANUAL Version 2.6.0*, J. F. Pelowitz (Editor), Los Alamos National Laboratory report, LA-CP-07-1473 (2008).

[13] L. Wolf, W. Scherer, et al., "High Temperature Reactor Core Physics and Reactor Dynamics," *Nucl. Eng. and Des.*, **121**, 227-240 (1990).

[14] P.E. MacDonald, J.W. Sterbentz, R.L. Sant, H.D. Gougar, R.L.Moore, et al., *NGNP Preliminary Point Design Results of the Initial Neutronics and Thermal-Hydraulic Assessments*, INEEL/EXT-03-00870 Rev. 1 (2003).

[15] P. Billot1, D. Barbier, "Very High Temperature Reactor," *Proc. of 2nd International Topical Meeting on High Temperature Reactor Technology*, Beijing, China (2004).

[16] G. Constantinescu, M. Chapelet, K. Squires, "Turbulence Modeling Applied to Flow over a Sphere," *AIAA Journal*, **41**, 9, 1733-1742 (2003).